Title

Regional heterogeneity of early GABAergic interneuron excitation *in vivo*

Author

Yasunobu Murata and Matthew T Colonnese

Affiliations

Department of Pharmacology and Physiology, and Institute for Neuroscience, George Washington University, 2300 Eye Street NW, Washington, DC 20037, USA

Corresponding authors:

Dr. Yasunobu Murata (murata@gwu.edu) and Dr. Matthew T Colonnese (colonnese@gwu.edu)

Abstract

GABA is thought to be excitatory during development but this is controversial, and the role of GABAergic transmission by interneurons *in vivo* remains unclear. In unanesthetized neonatal mice we show that postnatal day 3 (P3) GABAergic hippocampal neurons cause local excitation in CA1, which switches to inhibition by P7. By contrast, cortical interneurons cause inhibition at both ages. Thus, GABAergic excitation during development *in vivo* is age and region-specific.

Body

The developing brain spontaneously generates region- and age-specific activity, which is fundamental to circuit formation (Kirkby et al., 2013). Delayed expression of the neuronal K-Cl co-transporter KCC2 during development renders $GABA_A$ receptors depolarizing, and sometimes excitatory, in excised tissue preparations during this period. This early excitatory action of GABAergic neurons is hypothesized to drive activity and support glutamatergic and GABAergic synapse formation (Ben-Ari et al., 1997; Oh et al., 2016; Rivera et al., 1999). Recent studies *in vitro* (Dzhala et al., 2012) and *in vivo* (Kirmse et al., 2015; Valeeva et al., 2016) have questioned the generality of excitatory GABA. Furthermore, how local GABAergic interneurons regulate cortical excitability has not been directly measured *in vivo* (Kirmse et al., 2018), leaving obscure the role of interneurons in the generation of early activity *in vivo*.

To address this, we used a chemogenetic approach to bi-directionally modulate GABAergic interneuron excitability in unanesthetized neonatal mice while locally measuring network activity with extracellular electrodes. Local expression of chemogenetic receptors in GABAergic neurons was achieved by injecting cre-dependent adeno-associated virus encoding the inhibitory kappa-opioid receptor Designer Receptors Exclusively Activated by Designer Drugs (KOR-DREADD or KORD) (Vardy et al., 2015) or the excitatory DREADD (hM3Dq) (Armbruster et al., 2007) into hippocampus or visual cortex of GAD2-cre mice (Taniguchi et al., 2011) on the day of birth (P0). Both KORD and hM3Dq could be detected by P3. In both structures, expression was limited to GABAergic neurons (Fig.1a-b & Fig.3a-b). Whole-cell current-clamp recordings in slices showed hyperpolarization

by SalB (the KORD agonist) and depolarization by CNO (the hM3Dq agonist) in GABAergic neurons by P3 similar to that at P11 (Fig.1c & Fig.3c). Thus, this approach allowed for suppression (KORD-SalB) and enhancement (hM3Dq-CNO) of GABAergic neuronal activity in neonatal hippocampus and cortex.

To examine hippocampal activity, a 32-channel linear array was inserted into CA1 of dorsal hippocampus (Fig. 1d). As previously described, neuronal firing was largely restricted to the pyramidal cell layer and occurred almost entirely during early sharp waves (eSPWs), a developmentally-transient burst driven by cortical input transmitted through the entorhinal cortex (Leinekugel et al., 2002; Mohns and Blumberg, 2010; Valeeva et al., 2019) (Fig.1e). Only animals with viral expression surrounding the recording electrode and limited to hippocampus were analyzed. Suppressing the excitability of hippocampal GABAergic neurons by subcutaneous injection of SalB decreased multi-unit activity (MUA) in the pyramidal cell layer relative to pre-injection baseline (Fig.1f). The amplitude and occurrence, but not the duration, of eSPWs, and the local field potential (LFP) spectra in a broad frequency range were also reduced (Fig.1f, Supplementary Fig.1c). By contrast, in different animals, enhancing GABAergic neuron excitability by injecting CNO increased pyramidal layer MUA but did not alter eSPW amplitude nor LFP power (Fig.1g, Supplementary Fig.1a-b). Neither saline injection into animals expressing KORD/hM3Dq, nor SalB or CNO injections into GFP-only mice, altered activity. Thus, GABAergic interneurons excite the hippocampal CA1 network, and this excitation amplifies spontaneous activity during early development.

Such net-excitatory action of GABAergic neurons was no longer observed at P7. At P7, decreasing GABAergic neuron excitability increased pyramidal layer firing rates and the power of 6-14Hz frequencies in the LFP without significantly changing the occurrence, duration or amplitude of eSPWs (Supplementary Fig.2a). Enhancing interneuron excitability decreased pyramidal-layer firing and reduced LFP power in a broad frequency range (Fig.2c) without significantly affecting the eSPW (Supplementary Fig.2b). At P11, modulating GABAergic neuronal activity had similar effects on firing rates and LFP power (Fig.2d-e).

These results demonstrate a reversal of hippocampal GABAergic interneuron function, from excitatory to inhibitory, between P3 and P7.

In contrast to hippocampus, reducing the excitability of cortical GABAergic interneurons at P3 increased MUA firing rates recorded within the injected area (Fig.3d-e), while increasing their excitability had the opposite effects (Fig.3g). Neither manipulation significantly changed LFP spectral power, nor the occurrence, duration, or amplitude of spontaneous spindle-bursts (Supplementary Fig.3), the cortical activity driven by spontaneous retinal activity at this age (Hanganu et al., 2006). As in CA1, neither saline injection in DREADD expressing animals nor active drug in GFP expressing animals had an effect.

Modulation of GABA neuron excitability at P7 and at P11 had similar effects (Fig.3f, h). Thus, GABAergic interneurons have a net inhibitory role in visual cortex at ages at which they are excitatory in hippocampus.

Such regional heterogeneity of interneuron function suggests systemic modulations of GABAergic activity, as occurs in epilepsy treatment for example, would produce diverse outcomes. To examine this, we expressed KORD and hM3Dq in hippocampus as well as cortex, which provides the major drive to CA1 at these ages (Mohns and Blumberg, 2010; Valeeva et al., 2019), and recorded activity in the ipsilateral CA1 at P3. In contrast to injections limited to hippocampus, adding cortical suppression of GABAergic neuron excitability increased CA1 firing, while its enhancement reduced CA1 firing (Fig.4). Thus at P3, inhibition from interneurons in cortex can overwhelm local excitation by interneurons in hippocampus.

In hippocampus our *in vivo* results are consistent with recent *in vitro* recordings that show that $GABA_A$ receptors produce depolarization that increases principal cell firing before P3. Inhibitory responses emerge by P6 in undamaged neurons (Dzhala et al., 2012; Valeeva et al., 2013). However, our results differ from *in vivo*

recordings that showed an increase in EPSP frequency when GABAergic neurons are driven optogenetically at P3 (Valeeva et al., 2016). This may be a result of off target stimulation of cortical interneurons as a pan-expression system of GAD2-ChR2 transgenic mice was used, because we show that cortical inhibition dominates hippocampal excitation in the intact network. Our cortical results are consistent with previous *in vivo* studies (Valeeva et al., 2016, Kirmse et al., 2015).

To our knowledge, our data provide the first *in vivo* evidence that GABAergic interneurons are excitatory in the neonatal brain, providing up to 50% of the drive in CA1. However, we also see excitation by GABA within a more restricted range of ages and regions than predicted by traditional slice recordings and KCC2 expression (Ikeda et al., 2003; Rivera et al., 1999). Such heterogeneity is likely to exist among regions (Garaschuk et al., 2000), and within regions depending on neuronal birth-date (Yamada et al., 2004). Heterogeneity would be exacerbated by hormonal influence (Tyzio et al., 2006), epilepsy (Marguet et al., 2015) and autism risk (He et al., 2014; Tyzio et al., 2014). Finally, while we show strong regulation of excitability by GABAergic interneurons in developing networks, our results suggest that excitatory GABA is not a major contributor to the network dynamics of developing hippocampal and thalamocortical circuits (Colonnese and Phillips, 2018).

Figures

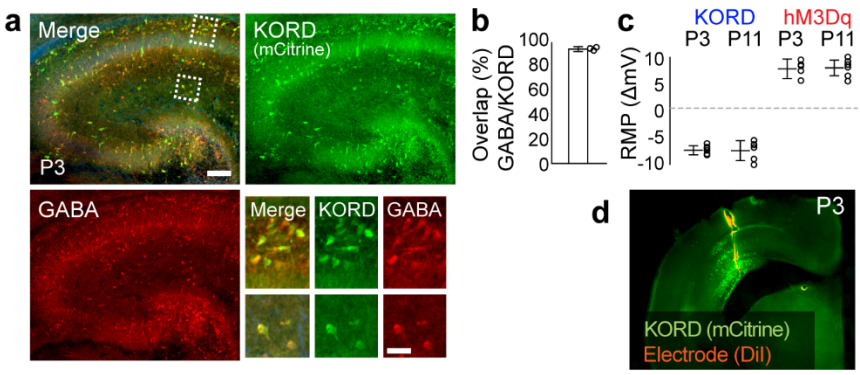
a
Merge
P3
KORD
(mCitrine)
GABA
Merge
KORD
GABA
b
Overlap (%)
GABA/KORD
100
80
60
40
20
0
c
KORD
hM3Dq
P3
P11
P3
P11
RMP (ΔmV)
10
5
0
-5
-10
d
P3
KORD (mCitrine)
Electrode (DiI)

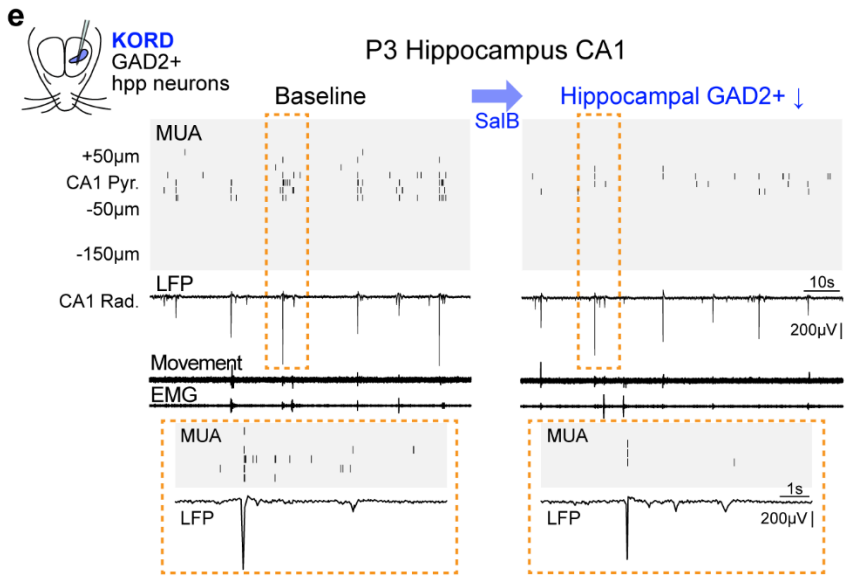
e
KORD
GAD2+
hpp neurons
P3 Hippocampus CA1
Baseline
SalB
Hippocampal GAD2+ ↓
MUA
+50μm
CA1 Pyr.
-50μm
-150μm
LFP
CA1 Rad.
10s
200μV
Movement
EMG
MUA
LFP
MUA
1s
LFP
200μV

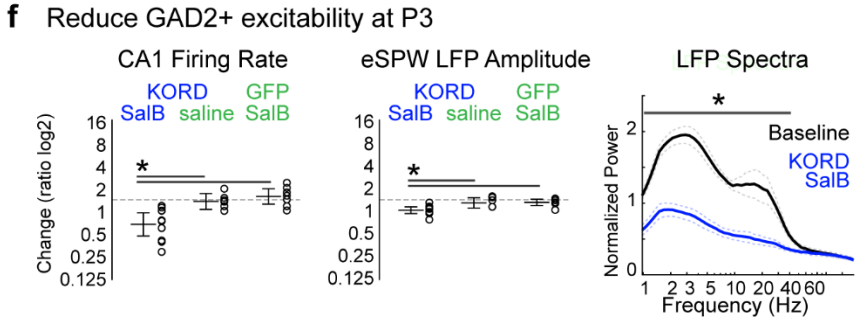
f
Reduce GAD2+ excitability at P3
CA1 Firing Rate
KORD
SalB
saline
GFP
SalB
Change (ratio log2)
16
8
4
2
1
0.5
0.25
0.125
*
eSPW LFP Amplitude
KORD
SalB
saline
GFP
SalB
*
LFP Spectra
*
Baseline
KORD
SalB
Normalized Power
2
1
0
1
2 3 5 10 20 40 60
Frequency (Hz)

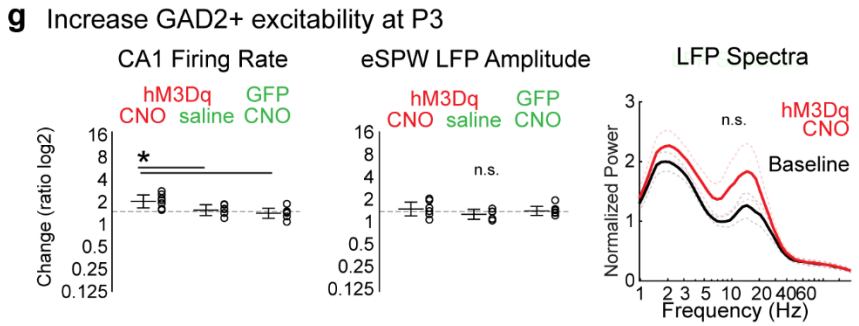
g
Increase GAD2+ excitability at P3
CA1 Firing Rate
hM3Dq
CNO
saline
GFP
CNO
Change (ratio log2)
16
8
4
2
1
0.5
0.25
0.125
*
eSPW LFP Amplitude
hM3Dq
CNO
saline
GFP
CNO
n.s.
LFP Spectra
n.s.
hM3Dq
CNO
Baseline
Normalized Power
3
2
1
0
1
2 3 5 10 20 40 60
Frequency (Hz)

Fig. 1: GABAergic interneurons are excitatory in 3-day old hippocampus *in vivo*. (a) Co-labeling of AAV-FLEX-KORD-IRES-mCitrine expressed in GAD2-Cre mouse with anti-GABA to label GABAergic neurons. Scale bars: 100µm and 20 µm **(b)** Percentage of KORD expressing neurons that also express GABA in three regions (n=3, mean+/- 95%CI, 0.95±0.03). **(c)** Change in membrane potential upon agonist infusion for KORD and hM3Dq expressing CA1 neurons at P3 and P11 (n=6,6,5,7; mean +/- 95%CI, -7.43±0.86, -7.5±1.89, 7.92±1.84, 8.09±1.46). **(d)** Representative localization of electrode and viral expression in P3 animal. **(e)** Representative recording for P3 reduction of GABAergic neuron excitability. Multi-unit spike activity (MUA) of spontaneous activity in CA1 hippocampus, along with associated *stratum radiatum* local field potential (LFP) and thoracic movement detection and electromyography (EMG). Activity is dominated by early sharp waves (eSPW) whose spike density is reduced following subcutaneous SalB (KORD agonist) injection. **(f)** Quantification of KORD-induced suppression of GABAergic neuron excitability and control conditions. From left: change in pyramidal cell layer firing rate (n=10,6,8; log2 ratio, mean +/- 95%CI: -1.23±0.58, -0.08±0.4, 0.17±0.39; ANOVA for manipulation, $p<0.001$), change in eSPW amplitude (-0.53±0.17, -0.16±0.26, -0.13±0.16; $p=0.002$), and normalized (to mean of 1-100Hz baseline) spectral power for *stratum radiatum* LFP (n=10, permutation test, $p<0.05$ at 1.0-48.7Hz). **(g)** Quantification of hM3Dq induced increase in GABAergic excitability (n=7,6,6; 0.51±0.33, 0.07±0.28, -0.09±0.25; $p=0.005$; 0.13±0.35, -0.14±0.25, 0.03±0.23; $p=0.33$; n=7, n.s. for all Hz).

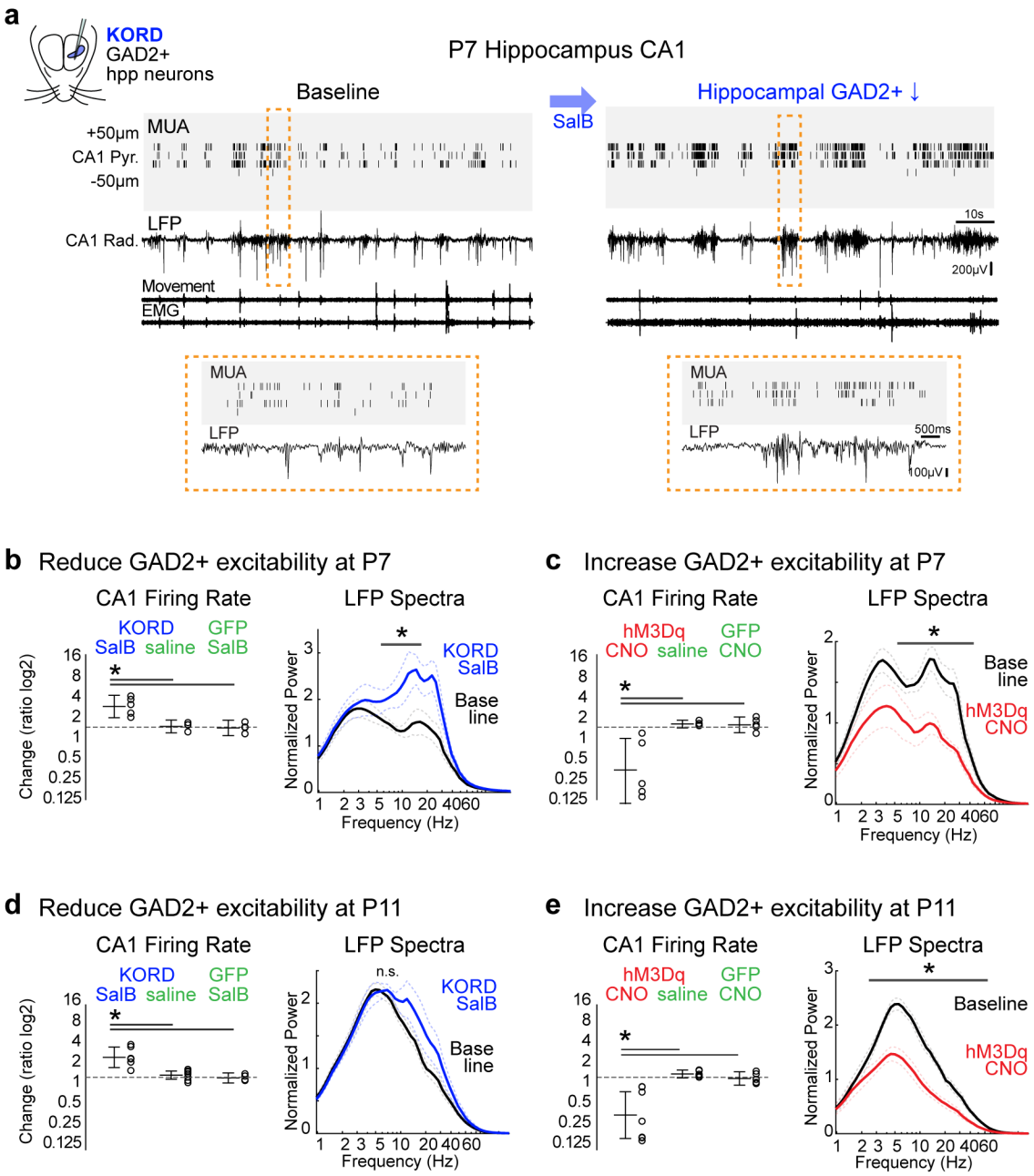

Fig. 2: Hippocampal GABAergic neurons are inhibitory by P7. (a) Representative recording for GABAergic neuron suppression in P7 hippocampus. **(b-c)** Quantification of suppression (b) and enhancement (c) of GABAergic neuron excitability at P7 (b: n=5,4,4; 1.14±0.62, 0.04±0.35, -0.04±0.43; p=0.001; n=5, p<0.05 at 6.9-14.7 Hz; c: n=5,4,5; -2.37±2.02, 0.17±0.21, 0.13±0.43; p=0.003; n=5, p<0.05 at 7.7-93.3 Hz). **(d-e)** Similar quantification at P11 (d: n=6,8,4; 1.11±0.57, 0.12±0.22, -0.03±0.28; p<0.001; n=6, n.s; e: n=7,5,5; -2.09±1.29, 0.18±0.22, -0.07±0.37; p=0.001; n=7 p<0.05 at 2.3-93.3 Hz).

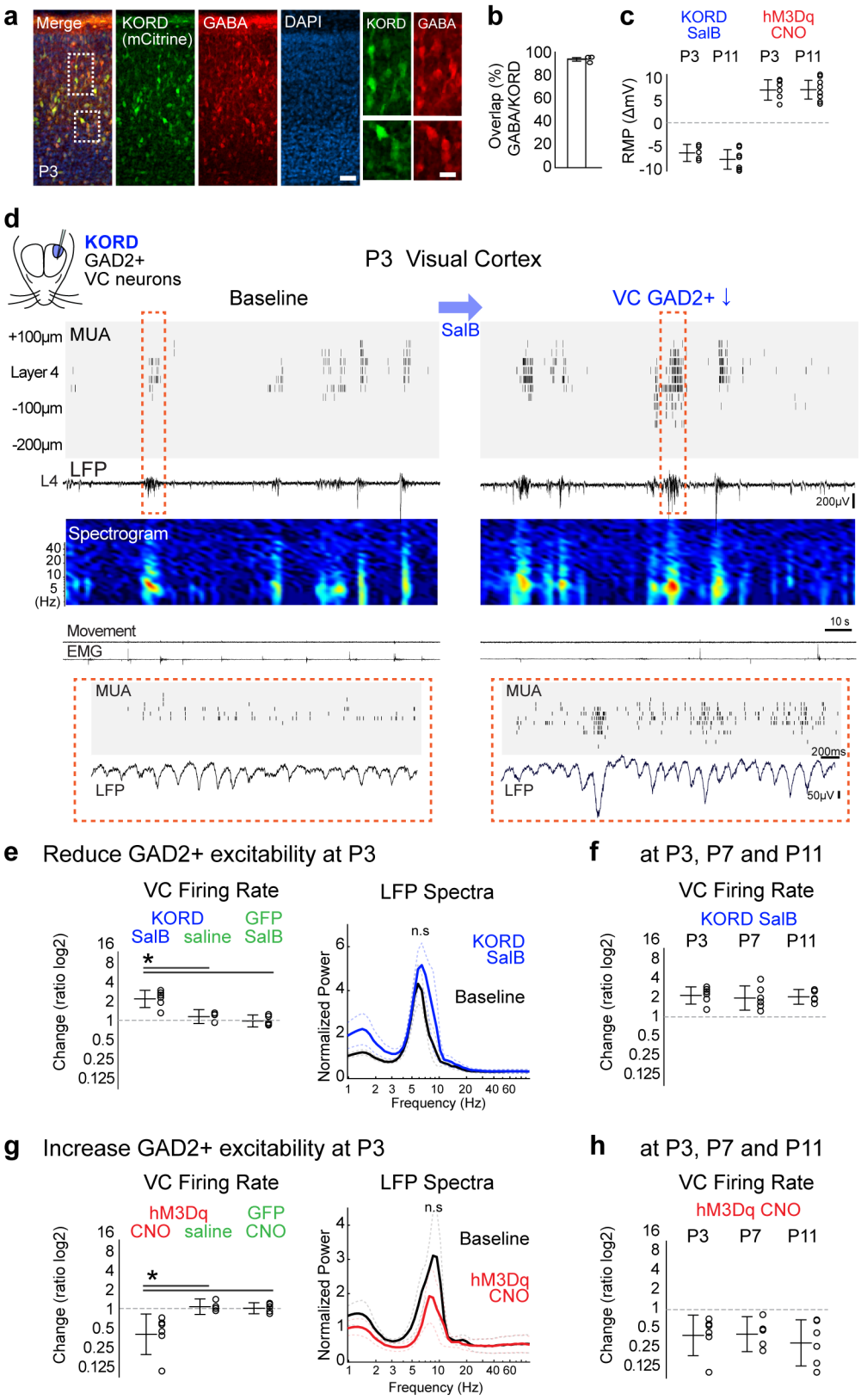

Fig. 3: GABAergic neurons in visual cortex have a net inhibitory action as early as P3. (a-b) Co-localization of KORD expression with GABA (n=3, 0.94±0.07). Scale bars: 50µm and 10 µm. **(c)** Change in membrane potential of GAD2+ neurons by activation of KORD and hM3Dq at P3 and P11 in visual cortical slices (n=5,7,6,8; -6.62±1.88, -

8.03±2.14, 7.18±2.23, 7.23±2.06). **(d)** Representative recording of visual cortex at P3 and the effect of GABAergic neuron suppression. LFP spectrogram is from presumptive layer 4. **(e)** Quantification of change in superficial layer firing rate (n=6,4,5; 1.25±0.5, 0.22±0.4, -0.03±0.35; p=0.001) and LFP spectral power (n=6; n.s.) following suppression of GABAergic neuron excitability by KORD activation. **(f)** Firing rate change at P3, P7 and P11 to KORD activation (n=6,6,5; 1.25±0.5, 1.11±0.71, 1.17±0.43; p=0.89). **(g-h)** As *e-f* but for GABAergic neuron enhancement by hM3Dq activation (g: n=6,4,5; -1.51±1.18, 0.11±0.46, 0.02±0.32; p=0.007, n=6, n.s.; h: n=5,6,7; -1.51±1.18, -1.43±1.02, -1.94±1.35; p=0.71).

Fig. 4

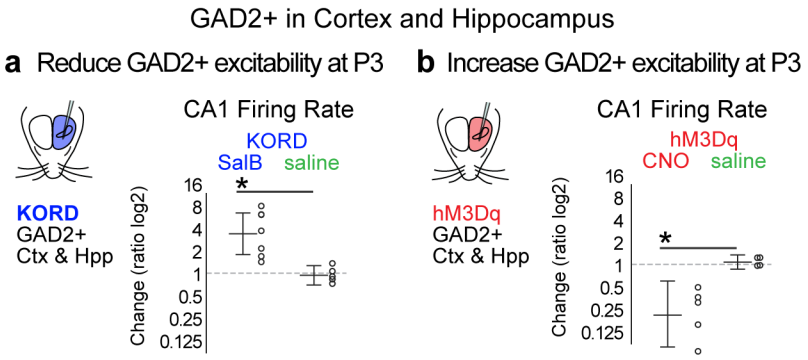

Fig. 4: GABAergic inhibition in cortex swamps local GABAergic excitation in hippocampus. (a) Change in CA1 pyramidal cell firing following suppression of GAD2+ neurons expressing KORD in both hippocampus and cortex at P3 (n=7, 5; 1.98±0.94, -0.11±-0.59; p=0.003). **(b)** Activation by hM3Dq (n=5, 4; -2.56±1.85, 0.11±0.36; p=0.01). Note both changes are opposite that observed for local viral expression (Fig.1).

Reference

Armbruster, B.N., Li, X., Pausch, M.H., Herlitze, S., and Roth, B.L. (2007). Evolving the lock to fit the key to create a family of G protein-coupled receptors potently activated by an inert ligand. Proc. Natl. Acad. Sci. *104*, 5163–5168.

Ben-Ari, Y., Khazipov, R., Leinekugel, X., Caillard, O., and Gaiarsa, J.-L. (1997). GABAA, NMDA and AMPA receptors: a developmentally regulated `ménage à trois'. Trends Neurosci. *20*, 523–529.

Colonnese, M.T., and Phillips, M.A. (2018). Thalamocortical function in developing sensory circuits. Curr. Opin. Neurobiol. *52*, 72–79.

Dzhala, V., Valeeva, G., Glykys, J., Khazipov, R., and Staley, K. (2012). Traumatic Alterations in GABA Signaling Disrupt Hippocampal Network Activity in the Developing Brain. J. Neurosci. *32*, 4017–4031.

Garaschuk, O., Linn, J., Eilers, J., and Konnerth, A. (2000). Large-scale oscillatory calcium waves in the immature cortex. Nat. Neurosci. *3*, 452.

Hanganu, I.L., Ben-Ari, Y., and Khazipov, R. (2006). Retinal Waves Trigger Spindle Bursts in the Neonatal Rat Visual Cortex. J. Neurosci. *26*, 6728–6736.

He, Q., Nomura, T., Xu, J., and Contractor, A. (2014). The Developmental Switch in GABA Polarity Is Delayed in Fragile X Mice. J. Neurosci. *34*, 446–450.

Ikeda, M., Toyoda, H., Yamada, J., Okabe, A., Sato, K., Hotta, Y., and Fukuda, A. (2003). Differential development of cation-chloride cotransporters and Cl− homeostasis contributes to differential GABAergic actions between developing rat visual cortex and dorsal lateral geniculate nucleus. Brain Res. *984*, 149–159.

Kirkby, L.A., Sack, G.S., Firl, A., and Feller, M.B. (2013). A Role for Correlated Spontaneous Activity in the Assembly of Neural Circuits. Neuron *80*, 1129–1144.

Kirmse, K., Kummer, M., Kovalchuk, Y., Witte, O.W., Garaschuk, O., and Holthoff, K. (2015). GABA depolarizes immature neurons and inhibits network activity in the neonatal neocortex *in vivo*. Nat. Commun. *6*, 7750.

Kirmse, K., Hübner, C.A., Isbrandt, D., Witte, O.W., and Holthoff, K. (2018). GABAergic Transmission during Brain Development: Multiple Effects at Multiple Stages. The Neuroscientist *24*, 36–53.

Leinekugel, X., Khazipov, R., Cannon, R., Hirase, H., Ben-Ari, Y., and Buzsáki, G. (2002). Correlated Bursts of Activity in the Neonatal Hippocampus in Vivo. Science *296*, 2049–2052.

Marguet, S.L., Le-Schulte, V.T.Q., Merseburg, A., Neu, A., Eichler, R., Jakovcevski, I., Ivanov, A., Hanganu-Opatz, I.L., Bernard, C., Morellini, F., et al. (2015). Treatment during a vulnerable developmental period rescues a genetic epilepsy. Nat. Med. *21*, 1436.

Mohns, E.J., and Blumberg, M.S. (2010). Neocortical Activation of the Hippocampus during Sleep in Infant Rats. J. Neurosci. *30*, 3438–3449.

Oh, W.C., Lutzu, S., Castillo, P.E., and Kwon, H.-B. (2016). De novo synaptogenesis induced by GABA in the developing mouse cortex. Science *353*, 1037–1040.

Rivera, C., Voipio, J., Payne, J.A., Ruusuvuori, E., Lahtinen, H., Lamsa, K., Pirvola, U., Saarma, M., and Kaila, K. (1999). The K + /Cl − co-transporter KCC2 renders GABA hyperpolarizing during neuronal maturation. Nature *397*, 251.

Taniguchi, H., He, M., Wu, P., Kim, S., Paik, R., Sugino, K., Kvitsani, D., Fu, Y., Lu, J., Lin, Y., et al. (2011). A Resource of Cre Driver Lines for Genetic Targeting of GABAergic Neurons in Cerebral Cortex. Neuron *71*, 995–1013.

Tyzio, R., Cossart, R., Khalilov, I., Minlebaev, M., Hübner, C.A., Represa, A., Ben-Ari, Y., and Khazipov, R. (2006). Maternal Oxytocin Triggers a Transient Inhibitory Switch in GABA Signaling in the Fetal Brain During Delivery. Science *314*, 1788–1792.

Tyzio, R., Nardou, R., Ferrari, D.C., Tsintsadze, T., Shahrokhi, A., Eftekhari, S., Khalilov, I., Tsintsadze, V., Brouchoud, C., Chazal, G., et al. (2014). Oxytocin-Mediated GABA Inhibition During Delivery Attenuates Autism Pathogenesis in Rodent Offspring. Science *343*, 675–679.

Valeeva, G., Valiullina, F., and Khazipov, R. (2013). Excitatory actions of GABA in the intact neonatal rodent hippocampus in vitro. Front. Cell. Neurosci. *7*.

Valeeva, G., Tressard, T., Mukhtarov, M., Baude, A., and Khazipov, R. (2016). An Optogenetic Approach for Investigation of Excitatory and Inhibitory Network GABA Actions in Mice Expressing Channelrhodopsin-2 in GABAergic Neurons. J. Neurosci. *36*, 5961–5973.

Valeeva, G., Janackova, S., Nasretdinov, A., Rychkova, V., Makarov, R., Holmes, G.L., Khazipov, R., and Lenck-Santini, P.-P. (2019). Emergence of Coordinated Activity in the Developing Entorhinal–Hippocampal Network. Cereb. Cortex *29*, 906–920.

Vardy, E., Robinson, J.E., Li, C., Olsen, R.H.J., DiBerto, J.F., Giguere, P.M., Sassano, F.M., Huang, X.-P., Zhu, H., Urban, D.J., et al. (2015). A New DREADD Facilitates the Multiplexed Chemogenetic Interrogation of Behavior. Neuron *86*, 936–946.

Yamada, J., Okabe, A., Toyoda, H., Kilb, W., Luhmann, H.J., and Fukuda, A. (2004). Cl− uptake promoting depolarizing GABA actions in immature rat neocortical neurones is mediated by NKCC1. J. Physiol. *557*, 829–841.

Supplementary information

Supplementary Figure 1

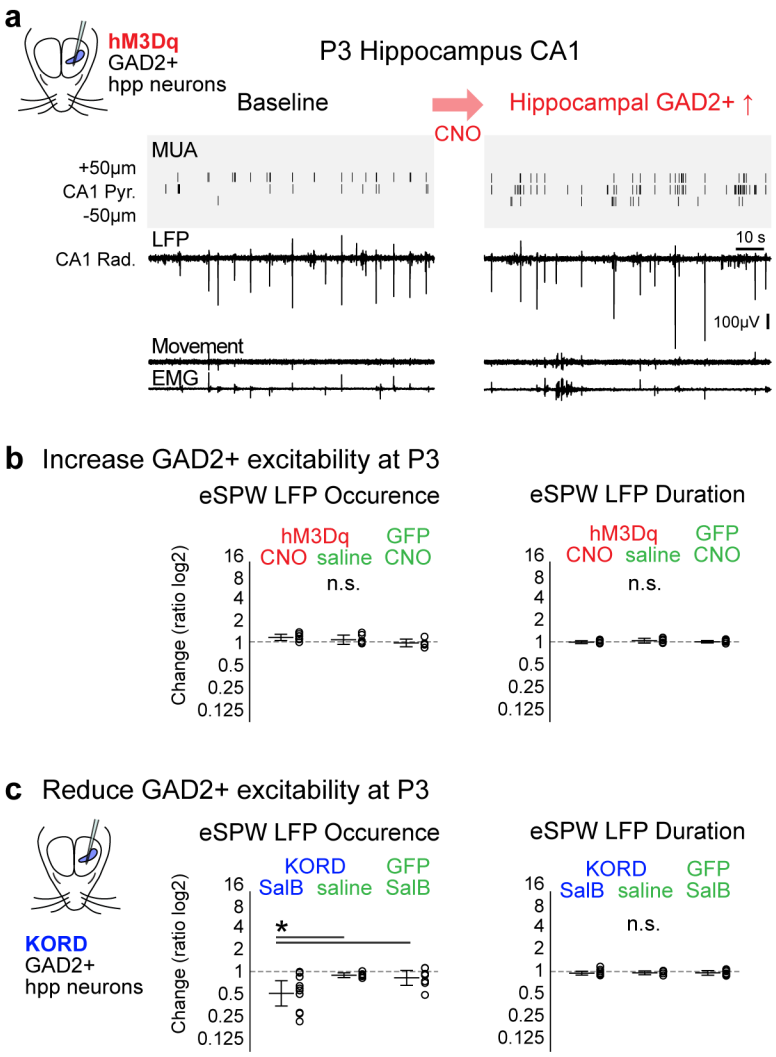

(a) Representative recording of hippocampus at P3 and the effect of GABAergic neuron enhancement. **(b)** Enhancement of hippocampal GABAergic neurons increases MUA firing rates (fig.1g) without significantly changing the amplitude (fig.1g), occurrence, and duration of eSPWs. (n=7,6,6, 0.22±0.16, 0.11±0.23, -0.05±0.19, p=0.0631; -0.01±0.07, 0.06±0.12, 0.01±0.06, p=0.2937) **(c)** Suppression of hippocampal GABAergic neurons increase MUA (fig.1f), the amplitude (fig.1f) and occurrence but not duration of eSPWs. (n=10,6,8, -1.09±0.64, -0.18±0.12, -0.31±0.37, p=0.0166; -0.08±0.1, -0.06±0.1, -0.07±0.11, p=0.9628)

Supplementary Figure 2

a Reduce GAD2+ excitability at P7

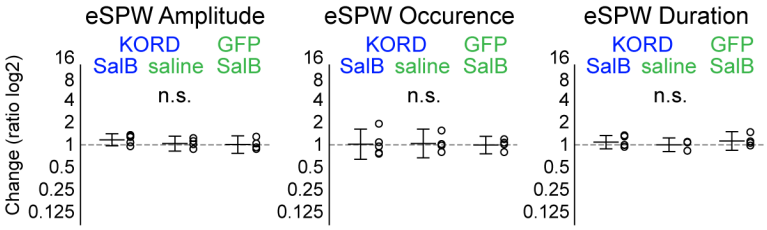

b Increase GAD2+ excitability at P7

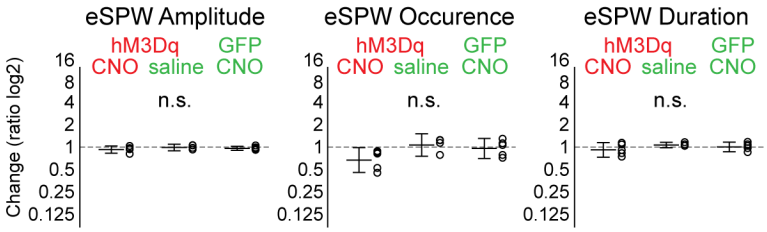

(a) Suppression of hippocampal GABAergic neurons at P7 increases MUA firing rates (fig.2b) without significantly changing the amplitude, occurrence, and duration of eSPWs. (n=5,4,4, 0.25±0.3, 0.06±0.37, 0.01±0.44, p=0.3491; 0.03±0.76, 0.06±0.72, -0.01±0.44, p=0.9754; 0.13±0.34, 0±0.34, 0.19±0.47, p=0.5855) **(b)** Enhancement of hippocampal GABAergic neurons at P7 increase MUA (fig.2c) without significantly changing the amplitude, occurrence and duration of eSPWs. (n=5,4,5; -0.12±0.18, -0.02±0.17, -0.06±0.1, p=0.4125; -0.65±0.63, 0.11±0.56, -0.06±0.5, p=0.0517; -0.14±0.36, 0.11±0.14, 0.01±0.24, p=0.2714)

Supplementary Figure 3

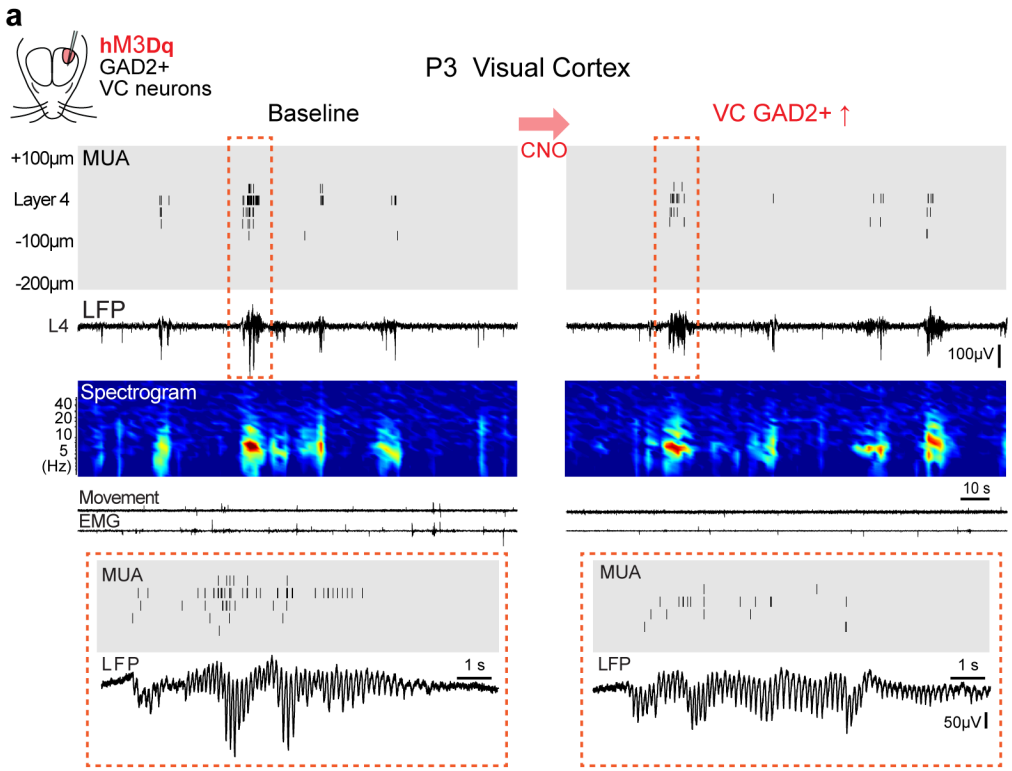

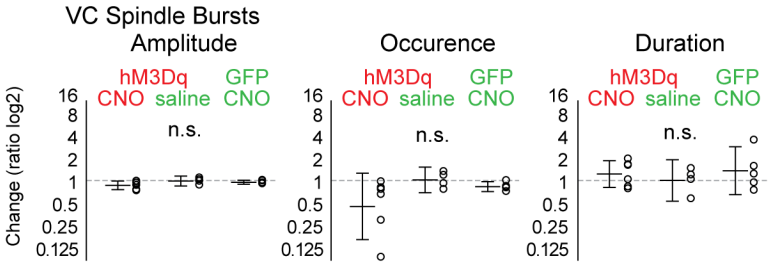

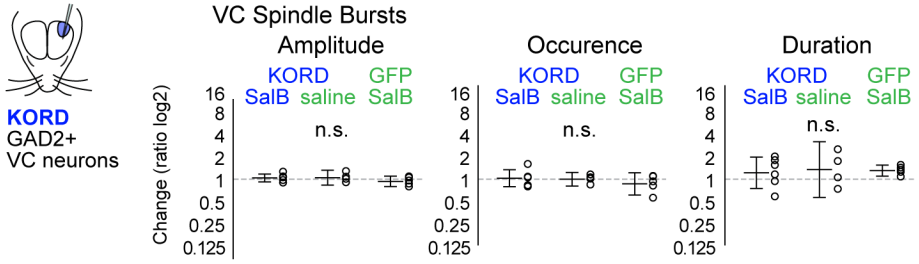

(a) Representative recording of visual cortex at P3 and the effect of GABAergic neuron enhancement. **(b)** Enhancement of visual cortical GABAergic neurons decreases MUA firing rates (fig. 3g) without significantly changing the amplitude, occurrence, and duration of spindle-burst oscillations. (n=6,4,5; -0.24±0.22, -0.02±0.25, -0.09±0.1, p=0.1267; -1.3±1.67 0.03±0.65, -0.31±0.25, p=0.1495; 0.33±0.67, 0.01±1.04, 0.49±1.21, p=0.6455) **(c)** Suppression of visual cortical GABAergic neurons increase MUA (fig. 3e) without significantly changing the

properties of spindle-burst. (n=6,4,5; 0.06±0.19, 0.07±0.37, -0.11±0.26, p=0.3256; 0.04±0.43, -0.01±0.34, -0.24±0.56, p=0.4675; 0.32±0.79, 0.48±1.4, 0.43±0.28, p=0.9292)

Supplementary Methods

In vivo recording

All experiments were conducted with approval from The George Washington University School of Medicine and Health Sciences Institutional Animal Care and Use Committee, in accordance with the *Guide for the Care and Use of Laboratory Animals* (NIH).

GAD2-IRES-Cre mice (Gad2$^{tm2(cre)Zjh}$) (Taniguchi et al., 2011) were acquired from The Jackson Laboratory (Stock No: 010802). C57BL/6 mice were acquired from The Jackson Laboratory and Hilltop Lab Animals. All GAD2-cre mice used were heterozygous, obtained by crossing homozygous GAD2-cre males and C57BL/6 females. Animals were housed one litter per cage on a 12/12 light/dark cycle. Both males and females were used.

In vivo recording methods are described previously (Murata and Colonnese, 2018; Shen and Colonnese, 2016). Topical lidocaine (2.5%) and systemic Carprofen (5 mg/kg) were used for preoperative analgesia. To place the headplate, under isoflurane anesthesia (3% induction, 0.5–1.5% maintenance, verified by toe pinch), the scalp was resected, the skull cleaned, and a stainless plate with a hole was placed so that the region over occipital cortex and hippocampus was accessible. The plate was fixed to the skull with vetbond and dental cement. Pups were monitored for signs of stress after recovery from anesthesia. For recording, the animal was head-fixed, and the body was supported within a padded enclosure. Body temperature was monitored with a thermocouple placed under the abdomen and maintained at 34–36°C by heating pad placed under the body restraint. Body movement was detected using a piezo-based detector placed under the enclosure. Electromyogram (EMG) was recorded from the ventral neck by a single stainless steel wire electrode. An Ag/AgCl wire was placed through the skull over Cerebellum as ground.

A variety of single and multi-shank silicon polytrodes (Neuronexus) were used, including 32-channel linear "edge" arrays with 100, 50, or 20 µm contact separation, and the "Poly2" configuration with two parallel rows with 50 µm separation. Electrodes were coated with DiI (Life Technologies) before insertion for histological verification of electrode location.

For VC recording, the monocular primary visual cortex was targeted with the following coordinates: -0.2~+0.2 mm anterior, 1.5~2.1mm lateral from the lambda at P3; -0.2~+0.2mm and 1.7~2.3mm at P7; and -0.2~+0.2mm and 2.1~2.9mm at P11. For hippocampal recording, the dorsal CA1 was targeted with the following coordinates: 0.5~0.8 mm anterior and 1.3~1.7mm lateral from the lambda at P3; 0.7~1.0mm and 1.4~1.9mm at P7; and 0.9~1.5mm and 1.7~2.3mm at P11.

SalB (1mg/kg, 0.1mg/ml in saline with 1% dimethyl sulfoxide (DMSO)) was subcutaneously injected to activate KORD, and CNO (10mg/kg; 1mg/ml in saline with 1% DMSO) was subcutaneously injected to activate hM3Dq (Vardy et al., 2015). Saline with 1% DMSO was subcutaneously injected as control.

Electrical signals were digitized using the Neuralynx Digital Lynx S hardware with Cheetah v5.6 software. dEEG signals were bandpass filtered between 0.1 Hz and 9 kHz, and digitized at 32 kHz. Cortical recordings were referenced to a contact site located in the underlying white matter. Hippocampus recordings were referenced to a contact just dorsal to hippocampus. Multiunit activity (MUA) was extracted by threshold crossing of −40 (P3) or -50 (P7 & P11) µV following 300 Hz to 9 kHz bandpass filtering.

Analysis

Neural signals were imported into MATLAB (MathWorks). Spike-times and dEEG were downsampled to 1 kHz. Before analysis, six animals were excluded for unstable baseline LFPs (periods with LFP amplitudes larger than

the maximum amplitude of visual response or with electrical or movement artifacts) or spike activity (more than 20% changes between the start and end of recording), eight animals were excluded for viral injection spread outside the recording region (hippocampus or visual cortex), and five animals were excluded because post-recording histology showed the electrode was not located in CA1 of the hippocampus.

For hippocampus, the pyramidal cell layer was identified in each recording as the channel with the highest MUA spike rate, and the *strata radiatum* was identified as the channel with largest negative LFP deflection. Average distance of the *strata radiatum* from the pyramidal cell layer was ~300µm at all ages. eSPWs were detected by identifying a triggering threshold of root mean square (RMS, 9ms window) of the strata radiatum LFP of 7 standard deviations above the mean. The beginning and end of the eSPW is defined as the points when the RMS remained above 2std and contained the initiation threshold.

For cortex, at P3 & P7, presumptive layer 4 was identified in each recording as the layer with the largest negative LFP deflection during spindle-bursts (Colonnese and Khazipov, 2010). In P11 animals, cortical layer 4 was identified in each recording as the channel with the earliest negative LFP deflection and the fastest spike response in the mean visual evoked response as previously described. (Colonnese and Khazipov, 2010; Shen and Colonnese, 2016). Spindle-bursts were identified by at least one negative trough of the layer 4 LFP that was greater than 5 std from the mean; additional cycles with negative LFP greater than 2 std within 1 second of each other were used to define the length of the burst.

For all analyses, after a one hour recovery period following electrode insertion, baseline activity was calculated from the entirety of a continuous 20 min period, while the experimental condition (KORD-SALB, KORD-saline, GFP-KORD, hM3Dq-CNO, hM3Dq-saline, GFP-CNO) was calculated from a 20 min period beginning 10 min after injection. For spectral analysis, LFP spectra from presumptive layer 4 (visual cortex) or *strata radiatum* (hippocampus) were obtained by averaging 2s multi-taper windows (time-band width 3 with 5 tapers (Chronux package (Mitra and Bokil, 2007)). To reduce the effect of the $1/f$ relationship, mean multitaper spectra were multiplied by frequency. The frequency axis was resampled on a log scale to equalize the representation of high and low frequencies and reduce the multiple-comparisons problem. For normalization, frequency power at each band was divided by the mean 1-100 Hz power of baseline.

Mean ± 95 % confidence interval are reported, and individual data were presented except for spectra. Hypothesis tests were conducted using nonparametric methods when $n < 10$. One-way ANOVA was used for all tests of manipulation and age dependence, and *post hoc* test (Tukey HSD) used to examine differences between specific manipulation and age groups. Significant differences by *post hoc* test ($p < 0.05$) are reported as asterisks on the relevant figure. P values <0.001 are rounded to nearest power of 10. Spectra were examined at each frequency for significant difference using nonparametric permutation tests corrected for multiple comparisons by the method of Cohen (Cohen, 2014) with $p < 0.05$. All tests were performed in MATLAB. The number of animals, the statistical test, results and p-values are reported in the supplemental table.

Virus injection

AAV8-hSyn-dF-HA-KORD-IRES-mCitrine (Vardy et al., 2015) and AAV8-hSyn-DIO-hM3D(Gq)-mCherry (Armbruster et al., 2007; Krashes et al., 2011) were obtained from Addgene (KORD: tier >7e12 GC/ml, Cat# 65417-AAV8; hM3Dq: tier >1e13 GC/ml, Cat#: 44362-AAV8), and AAV1-CAG-FLEX-GFP was obtained from The Penn Vector Core (tier >2.9e13 GC/ml, Cat#: AAV1-AllenInstitute854). Mouse pups at the day of birth (P0) were cold anesthetized, and 30–100 nl of viral solution was injected locally into the hippocampus (0.4-0.8mm anterior and 1.2-1.8mm lateral from the Lambda, 1.0-1.2mm depth) or visual cortex (-0.2-0.0 mm anterior and 1.5-2.0mm lateral from the Lambda, 0.4-0.7mm depth) using a Nanoject II (Drummond). Two days post injection yielded

visible expression of fluorophore around the injected sites. Expression local to the recording electrode and limited to the region of interest was verified in all animals recorded. About the half of animals were injected with only AAV-FLEX-GFP for control, and the rest were injected with AAV-dF-KORD and/or AAV-DIO-hM3Dq and/or AAV-FLEX-GFP. Recordings and analyses were conducted in a blind manner.

Slice recording

Slice recordings were conducted as previously described with slight modifications (Bolton et al., 2015; Zhao et al., 2013). Mice were anesthetized with Isoflurane and decapitated. The brain was quickly removed and placed in ice-cold cutting solution containing 110 mM Choline Chloride, 2.5 mM KCl, 25 mM $NaHCO_3$, 1.25 mM NaH_2PO_4, 12 mM glucose, 3 mM sodium pyruvate, 10 mM sodium ascorbate, 7 mM $MgSO_4$, and 0.5 mM $CaCl_2$. Coronal cortical and hippocampal slices (300 µm) were cut using a Leica Vibratome VT 1000S. The slices were kept in ACSF containing 127 mM NaCl, 2.5 mM KCl, 25 mM $NaHCO_3$, 1.25 mM NaH_2PO_4, 12 mM glucose, 1 mM $MgCl_2$, 2 mM $CaCl_2$ at 32 °C for at least 15 min then at room temperature (22 - 25 °C). Slices were placed in a recording chamber at room temperature and continuously perfused with carbogenated ACSF. pClamp 8.1 (Molecular Devices) was used to acquire and analyze data. Electrical signals were amplified with an Axopatch 200B amplifier, digitized with a Digidata 1322A interface (Molecular Devices), filtered at 2 kHz, sampled at 5 kHz.

Glass pipettes (2 - 6 MΩ) were filled with an internal solution containing the following: 105 mM K-gluconate, 10 mM Na-phosphocreatine, 4 mM EGTA, 10 mM HEPES, 4 mM Na-ATP, 1 mM Na-GTP, 3 mM $MgCl_2$, 0.07 mM $CaCl_2$, brought to ∼290 mOsm with ∼28 mM sucrose and pH 7.3 with KOH. GABAergic cortical and hippocampal neurons with fluorescence were patched under a 40x objective, and whole-cell current-cramp recordings were conducted to measure the changes in resting membrane potential following bath application of 100nM SalB or 100nM CNO. At least 1 minute of stable membrane potential was analyzed using Clampfit software (Molecular Devices) before and after treatment.

immunohistochemistry

Animals were perfused post-fixed with 4% Paraformaldehyde in PBS. Brains were sectioned by vibratome at 150µm in the coronal plane. For cryosectioning, brains were cryoprotected in 10% and 30% sucrose in PBS, then sectioned at 40µm. Following antibodies are used: rabbit anti-GABA (Sigma, A2052, Lot# 103M4793), chicken anti-GFP (Abcam, ab13970, Lot# GR3190550-12), mouse anti-RFP (Rockland, 200-301-379S, Lot 34356), anti-chicken Alexa 488, anti-mouse Alexa 555, anti-rabbit Alexa 488, anti-rabbit Alexa 555, DAPI (ThermoFisher). Confocal images were taken with Zeiss710 using a 10x objective, and analyzed with FIJI (ImageJ).

Reference

Armbruster, B.N., Li, X., Pausch, M.H., Herlitze, S., and Roth, B.L. (2007). Evolving the lock to fit the key to create a family of G protein-coupled receptors potently activated by an inert ligand. Proc. Natl. Acad. Sci. *104*, 5163–5168.

Bolton, A.D., Murata, Y., Kirchner, R., Kim, S.-Y., Young, A., Dang, T., Yanagawa, Y., and Constantine-Paton, M. (2015). A Diencephalic Dopamine Source Provides Input to the Superior Colliculus, where D1 and D2 Receptors Segregate to Distinct Functional Zones. Cell Rep. *13*, 1003–1015.

Cohen, M.X. (2014). Analyzing Neural Time Series Data (MIT Press).

Colonnese, M.T., and Khazipov, R. (2010). "Slow Activity Transients" in Infant Rat Visual Cortex:A Spreading Synchronous Oscillation Patterned by Retinal Waves. J. Neurosci. *30*, 4325–4337.

Krashes, M.J., Koda, S., Ye, C., Rogan, S.C., Adams, A.C., Cusher, D.S., Maratos-Flier, E., Roth, B.L., and Lowell, B.B. (2011). Rapid, reversible activation of AgRP neurons drives feeding behavior in mice. J. Clin. Invest. *121*, 1424–1428.

Mitra, P., and Bokil, H. (2007). Observed Brain Dynamics (Oxford, New York: Oxford University Press).

Murata, Y., and Colonnese, M.T. (2018). Thalamus Controls Development and Expression of Arousal States in Visual Cortex. J. Neurosci. *38*, 8772–8786.

Shen, J., and Colonnese, M.T. (2016). Development of Activity in the Mouse Visual Cortex. J. Neurosci. *36*, 12259–12275.

Taniguchi, H., He, M., Wu, P., Kim, S., Paik, R., Sugino, K., Kvitsani, D., Fu, Y., Lu, J., Lin, Y., et al. (2011). A Resource of Cre Driver Lines for Genetic Targeting of GABAergic Neurons in Cerebral Cortex. Neuron *71*, 995–1013.

Vardy, E., Robinson, J.E., Li, C., Olsen, R.H.J., DiBerto, J.F., Giguere, P.M., Sassano, F.M., Huang, X.-P., Zhu, H., Urban, D.J., et al. (2015). A New DREADD Facilitates the Multiplexed Chemogenetic Interrogation of Behavior. Neuron *86*, 936–946.

Zhao, J.-P., Murata, Y., and Constantine-Paton, M. (2013). Eye opening and PSD95 are required for long-term potentiation in developing superior colliculus. Proc. Natl. Acad. Sci. *110*, 707–712.